Electronic Supplementary Material (ESI) for ChemComm.

Supporting Information

All-Thiolate-Stabilized Ag_{42} Nanocluster with a Tetrahedral Kernel Bi-Tetrahedral Kernel

Tao Chen,‡ Sha Yang,‡ Yongbo Song,* Jinsong Chai, Qinzhen Li, Xiangyu Ma, Guang Li, Haizhu Yu,* Manzhou Zhu*

Table of Contents

Experimental Procedures

1. Chemicals:

All reagents and solvents were commercially purchased and used as received without further purification, including silver nitrate ($AgNO_3$, 99%), *tert*-butyl mercaptan (≥99.99%), cyclohexyl mercaptan (≥99.99%), 2-methyltetrahydrofuran (≥99.99%), glutathione (GSH, ≥99.99%) tetraoctylammonium chloride (TOACl, ≥99.99%), Sodium hexafluoro antimonate ($NaSbF_6$, ≥99.99%) sodium borohydride ($NaBH_4$, >98%), methanol (HPLC grade, ≥99.9%), dichloromethane (HPLC grade, ≥99.9%) and ethanol (HPLC grade, ≥99.9%). All glassware was cleaned with aqua regia (HCl: HNO_3 = 3:1 vol%), washed with copious nanopure water, and then dried in an oven prior to use.

Synthesis of nanoclusters $Ag_{42}(SBu^t)_{24}$.

$Ag_{42}(SBu^t)_{24}$ was synthesized by a two-step synthetic method.

(i) The synthesis of the precursor $Ag_m(SG)_n$. $AgNO_3$ (49.4 mg, 0.3 mmol) was first dissolved in 2 mL of water in a 50 mL single-neck round-bottom flask and then mixed with 8 mL of water. Then, GSH (200 mg, 0.65 mmol), $NaSbF_6$ (77.6 mg, 0.3 mmol) and NaOH (40mg, 1mmol) was added into the mixture. After about 20 min, 2 mL of $NaBH_4$ aqueous solution (18.0 mg/mL) was quickly added into solution under vigorous stirring. The color of the solution turned to yellow and then to black within about 1 min. The reaction was then continued for 3 hours. After that, the precursors were obtained.

(ii) Two-Phase Ligand Exchange. The obtained aqueous solution of $Ag_m(SG)_n$ was mixed with 15 mL CH_2Cl_2 and 2 mL tert-butyl mercaptan. The solution was reacted for 12 h at room temperature with vigorous stirring. The $Ag_m(SG)_n$ NCs were found to transfer from the aqueous phase to the organic phase. Then, water was removed, and the organic phase was washed with ethanol for three times to remove excess thiolate. The $Ag_{42}(SBu^t)_{24}$ NCs were then crystallized in CH_2Cl_2/CH_3OH, and black crystals were obtained after about one week.

Synthesis of nanoclusters $Ag_{61}(SC_6H_{11})_{40}Cl$.

The synthetic method of $Ag_{61}(SC_6H_{11})_{40}Cl$ was similar to that of $Ag_{42}(SBu^t)_{24}$. The first step (i.e. synthesis of the precursors) was the same, but tert-butyl mercaptan was replaced by cyclohexanethiol in the second step, and additional TOACl was added as Cl resources and to promote the phase transfer.

The transformation of Ag_{42} to Ag_{61} NCs

10 mg of $Ag_{42}(SBu^t)_{24}$ NCs was dissolved in 1 mL of dichloromethane (DCM), and 0.5 mL of cyclohexanethiol and 10 mg TOACl were added. After about 6 hours, the **Ag_{42}** was transformed to crude **Ag_{61}**, which was further purified by CH_2Cl_2/MeOH solvent to obtain **Ag_{61}** nanocluster.

2. Characterization:

The UV-Vis-NIR absorption spectra were recorded using an Agilent 8453 diode array spectrometer (in CH_2Cl_2, and 2-methyltetrahydrofuran was used for time-dependent UV-Vis tests), whose background correction was made using a CH_2Cl_2 and 2-methyltetrahydrofuran blank, accordingly. Solid samples were first dissolved in CH_2Cl_2 to make a dilute solution, with a subsequent transformation to a 1 cm path length quartz cuvette, followed by spectral measurements.

Thermogravimetric analysis (TGA) was carried out on a thermogravimetric analyzer (DTG-60H, Shimadzu Instruments, Inc.) with 10.4356 mg of the $Ag_{42}(SBu^t)_{24}$ and 12.5941 mg of the $Ag_{61}(SC_6H_{11})_{40}Cl$ NCs in a SiO_2 pan at a heating rate of 10 K/min from 283 K to 1073 K.

X-ray photoelectron spectroscopy (XPS) measurements were performed on a Thermo ESCALAB 250 configured with a monochromated AlKα (1486.8 eV) 150W X-ray source, 0.5 mm circular spot size, a flood gun to counter charging effects, and the analysis chamber base pressure lower than 1 x 10^{-9} mbar. Data were collected with FAT=20 eV.

Electrospray ionization mass spectra (ESI-MS) were recorded using a Waters UPLC H-class/Xevo G2-XS Qtof mass spectrometer. The sample was directly infused into the pump at 5 μL/min. ESI sample was prepared by dissolving in mixed solution of dichloromethane/methanol.

NMR measurements were performed on a JNM-ECZ600R instrument. The data was collected with ~20 mg nanocluster dissolved in 1mL CD_2Cl_2.

3. X-ray crystallographic determination of Ag_{42} and Ag_{61}.

The data collection for single crystal X-ray diffraction was carried out on a Bruker Smart APEX II CCD diffractometer at 296 K, using graphite-monochromatized Mo Kα radiation (λ = 1.54178 Å). Data reductions and absorption corrections were performed using the SAINT and SADABS programs, respectively. The structure was solved by direct methods and refined with full-matrix least squares on F^2 using the SHELXTL software package. All non-hydrogen atoms were refined

anisotropically. All hydrogen atoms were set in geometrically calculated positions and refined isotropically using a riding model.
Paragraph.

Results and Discussion

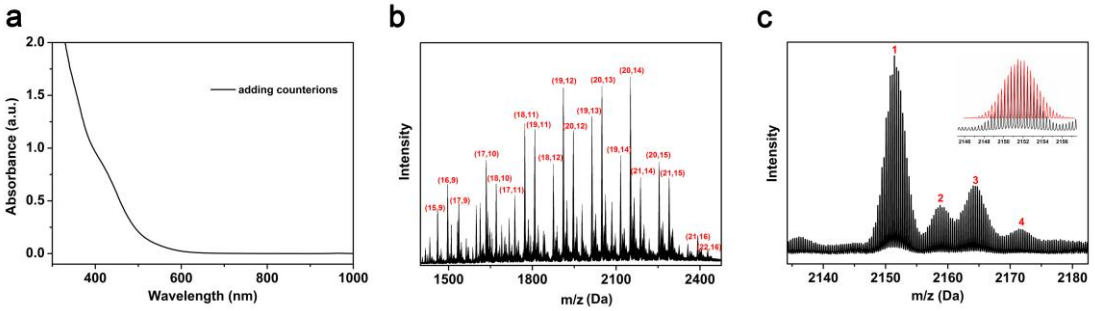

Figure S1. (a) UV-vis and (b) ESI-MS spectra of water-soluble precursor in presence of $NaSbF_6$, the numbers in parentheses denote the number of metals and ligands in nanoclusters, (c) the magnified view of the highest peak (20, 14), inset: experimental data (black) and the simulated spectra (red) for peak 1 (i.e. $[Ag_{20}(SG)_{14}\text{-}3H^+]^{3-}$), peak 2, 3, and 4 attributed to $[Ag_{20}(SG)_{14}+Na^+\text{-}4H^+]^{3-}$, $[Ag_{20}(SG)_{14}+K^+\text{-}4H^+]^{3-}$, and $[Ag_{20}(SG)_{14}+Na^+ +K^+\text{-}5H^+]^{3-}$.

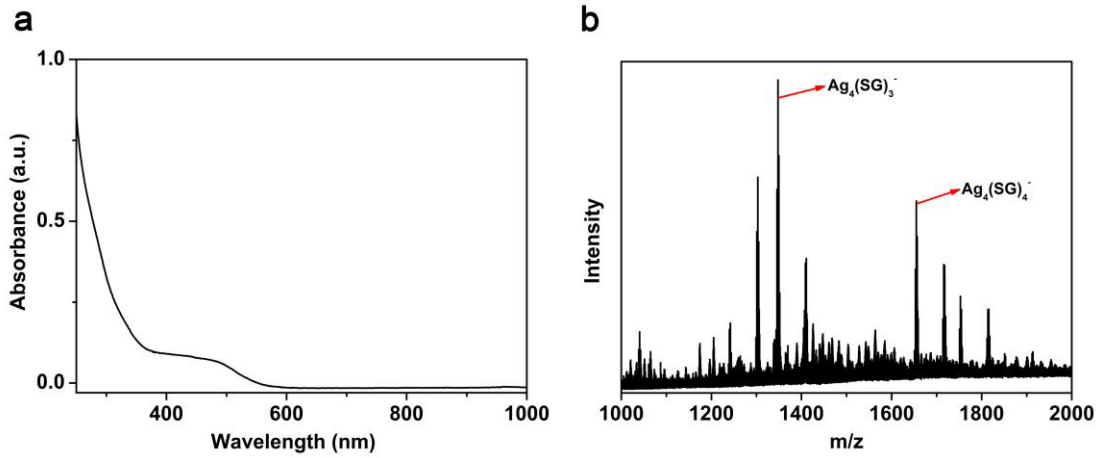

Figure S2. (a)UV-vis and (b) ESI-MS spectra of water-soluble precursors in the absence of $NaSbF_6$.

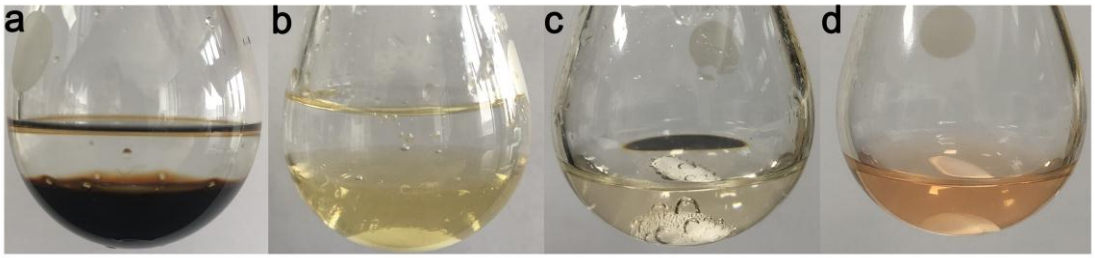

Figure S3. Digital photographs of products obtained by two phase ligand exchange (a) after adding $NaSbF_6$, and (b) $NaBPh_4$. The lower solution is dichloromethane and the upper solution is water. Under the same conditions, after adding (c) KPF_6 and (d) $NaAlF_6$, the color of the aqueous solution was light, indicating that the metal complexes were not reduced and cannot be used for ligand exchange.

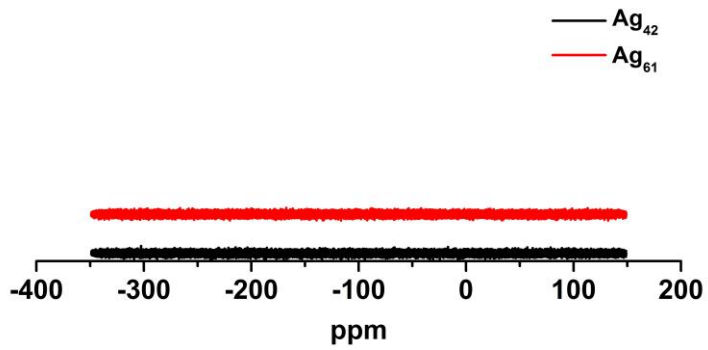

Figure S4. ^{19}F-NMR of **Ag_{42}** and **Ag_{61}**.

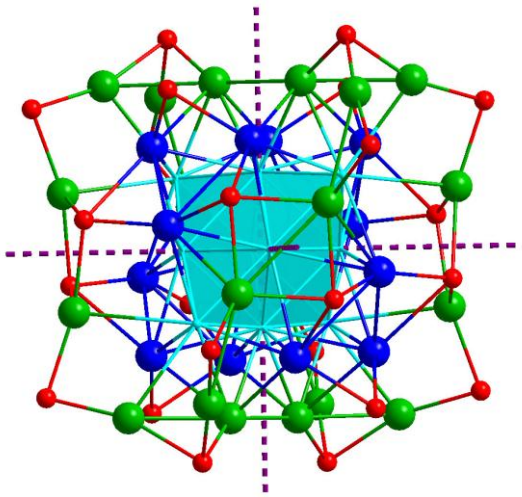

Figure S5. The total structure comparises three C_2 symmetry axis perpendicular to each other.

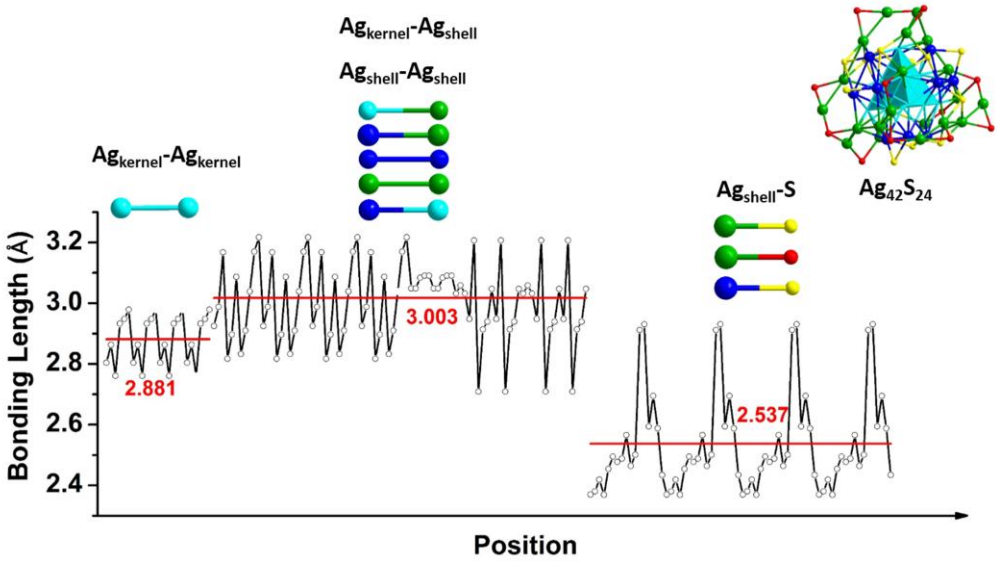

Figure S6. The bond length distributions in the **Ag$_{42}$** nanocluster. (Color labels: Ag, turquoise/green/blue; S, red/yellow; Cl, violet. For clarity, all C and H atoms are omitted).

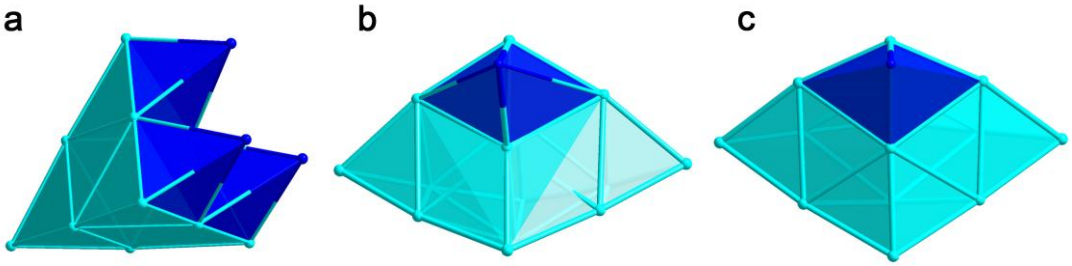

Figure S7. (a) The triangle growth of the kernel of **Ag$_{42}$**, and (b, c) the two face-fused bi-tetrahedron in **Ag$_{61}$**.

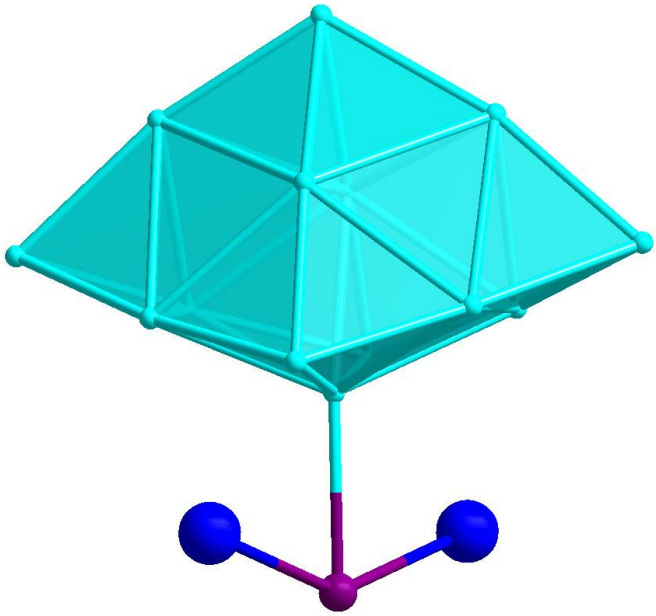

Figure S8. The binding mode of μ_3-Cl atom with the three neighboring silver atoms.

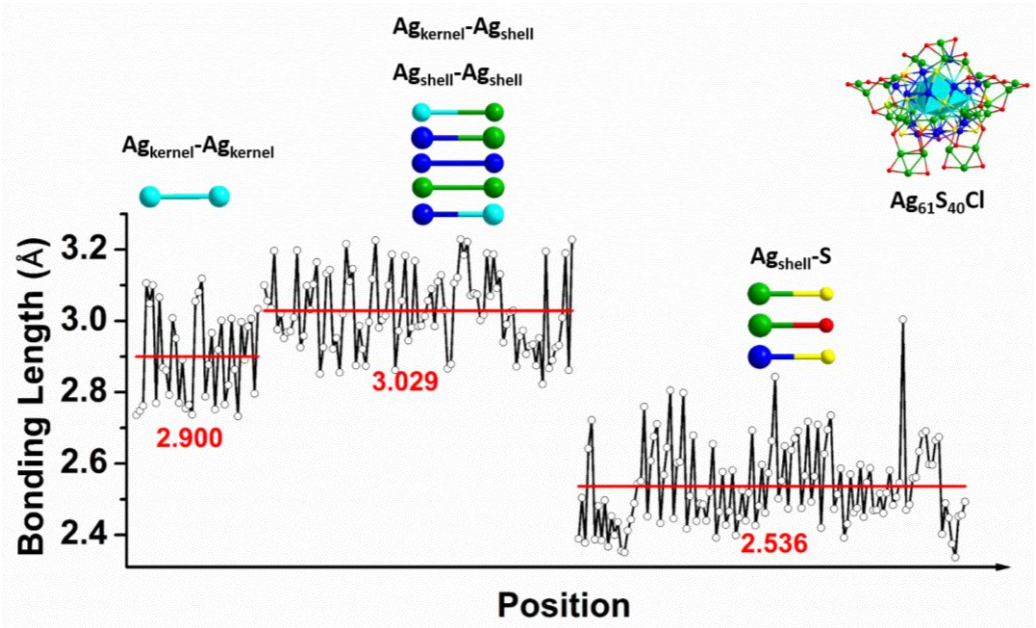

Figure S9. The bond length distributions in the **Ag$_{61}$** nanocluster. (Color labels: Ag, turquoise/green/blue; S, red/yellow; Cl, violet. For clarity, all C and H atoms are omitted).

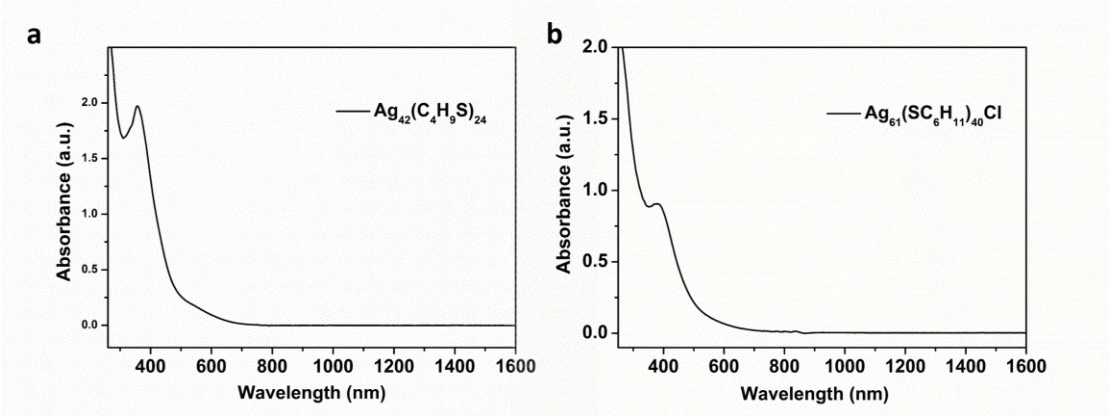

Figure S10. UV-vis-NIR spectra of (a) **Ag_{42}** and (b) **Ag_{61}** NCs.

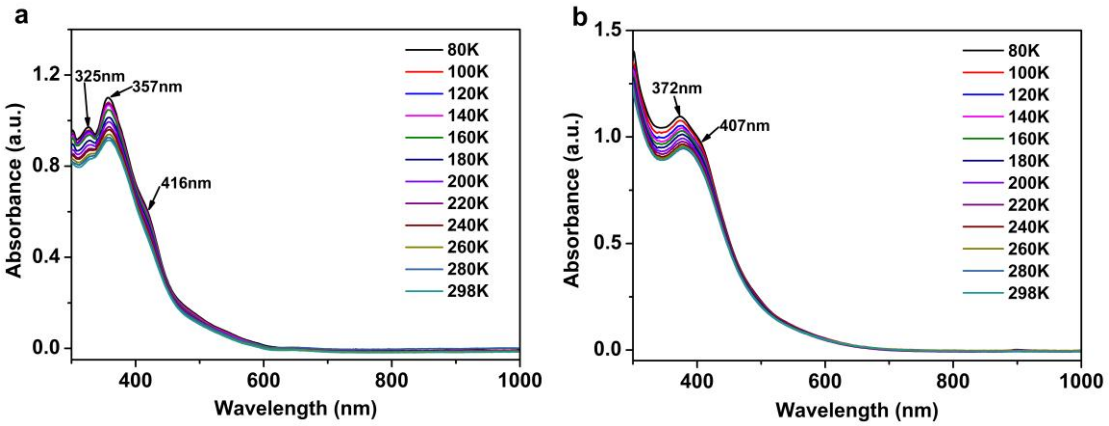

Figure S11. Temperature-dependent UV-vis spectra of (a) **Ag_{42}** and (b) **Ag_{61}** NCs dissolved in a 2-Methyltetrahydrofuran.

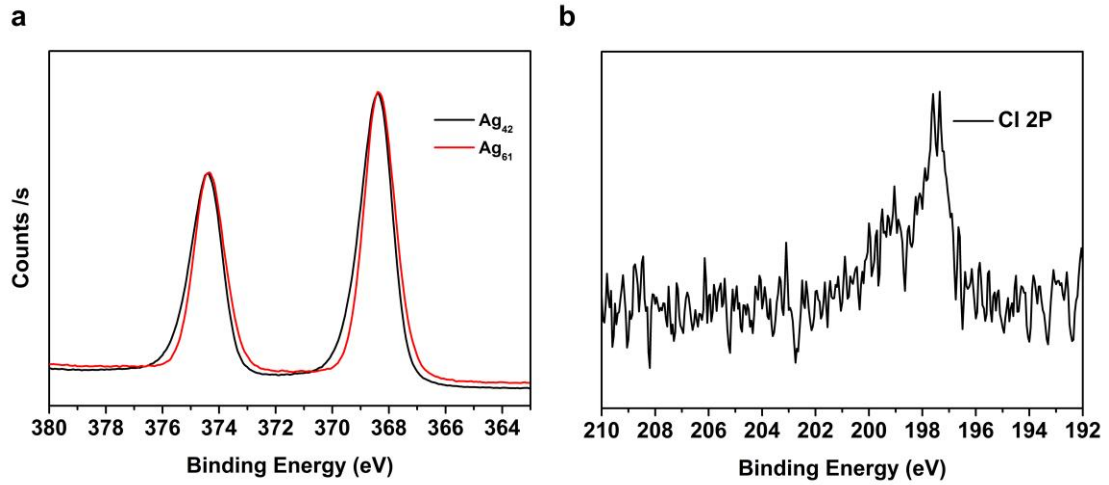

Figure S12. (a) Ag 3d XPS spectra of **Ag_{42}** and **Ag_{61}** NCs. (b) The Cl 2p spectra of **Ag_{61}** NCs.

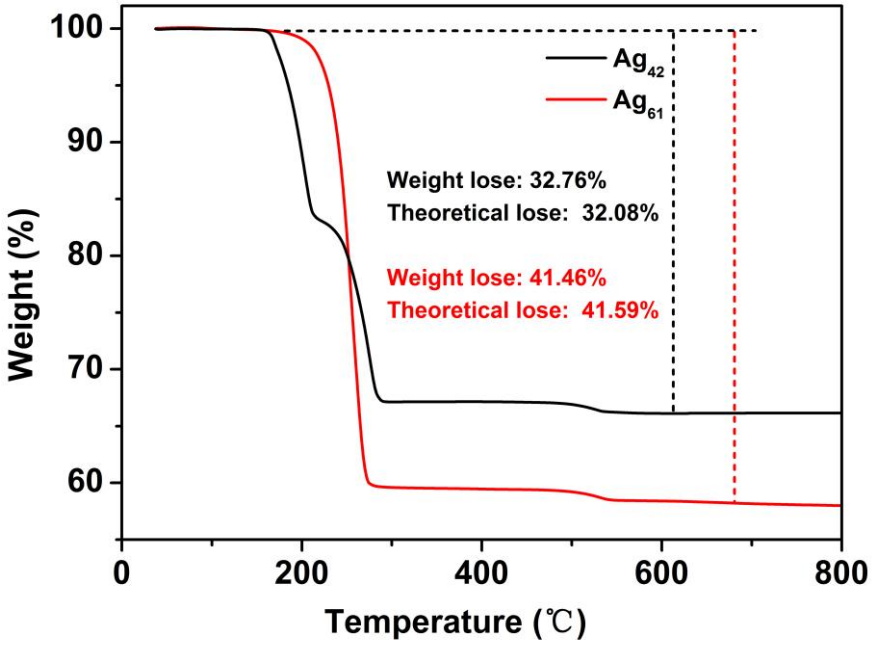

Figure S13. TGA of **Ag_{42}** and **Ag_{61}**.

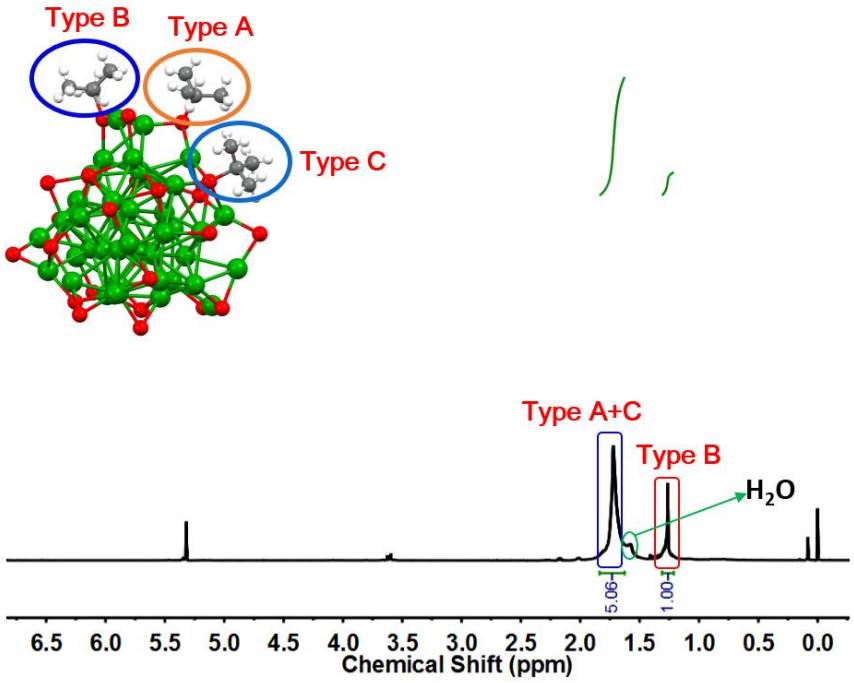

Figure S14. ^{1}H-NMR spectrum of the **Ag_{42}** nanocluster, **Ag_{42}** in CD_2Cl_2 showed two resonances (1.26 and 1.72 ppm) in a ratio of 1 : 5, which is consistent with the numbers of the types of ^{t}BuS- ligands (Type B : Type A+C = 4 : 20), and δ (1.54) is assigned to H_2O.

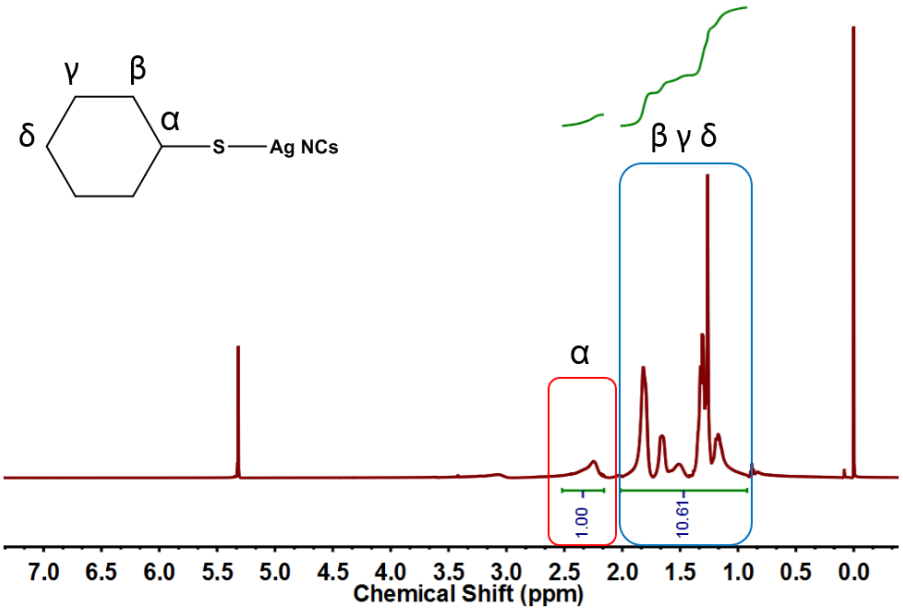

Figure S15. ^{1}H-NMR spectrum of the **Ag_{61}** nanocluster, the peaks at (2.12-2.51 ppm) are assigned to α-CH, the peaks at (0.93-2.05 ppm) mainly correspond to β-CH_2, γ-CH_2 and δ-CH_2 with integrals of 1:10.

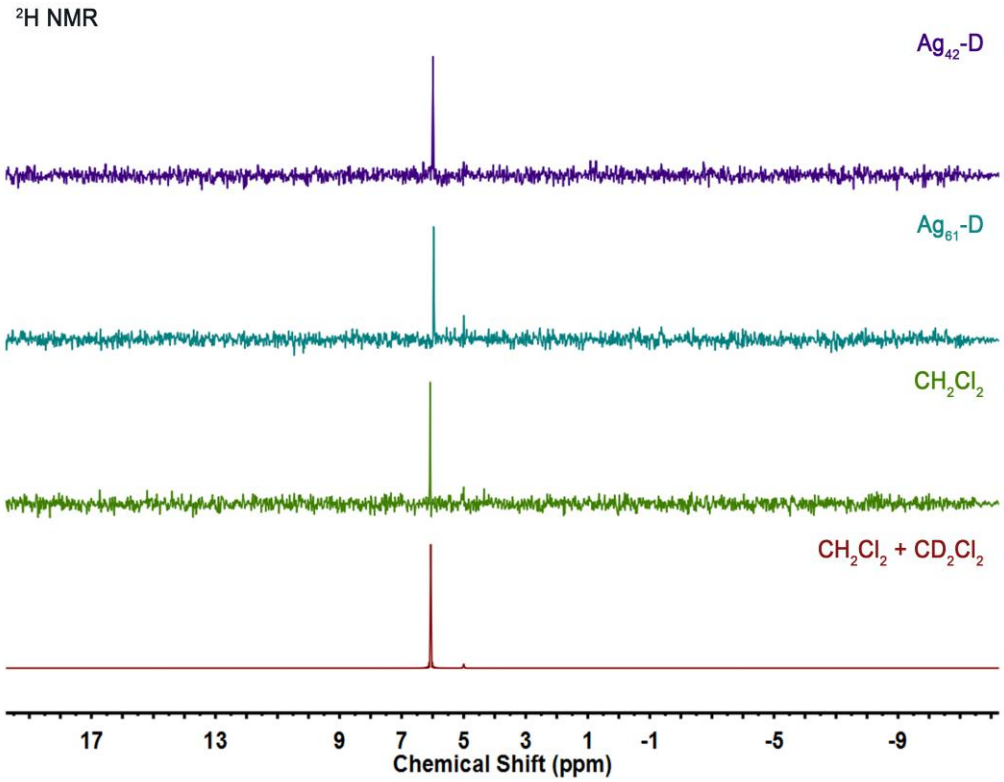

Figure S16. ^{2}H-NMR spectra of **Ag_{42}-D** (purple line), (b) **Ag_{61}-D** (teal line), CH_2Cl_2 (green line), (d) CH_2Cl_2 + CD_2Cl_2 (maroon line). (The solvent is dichloromethane.)

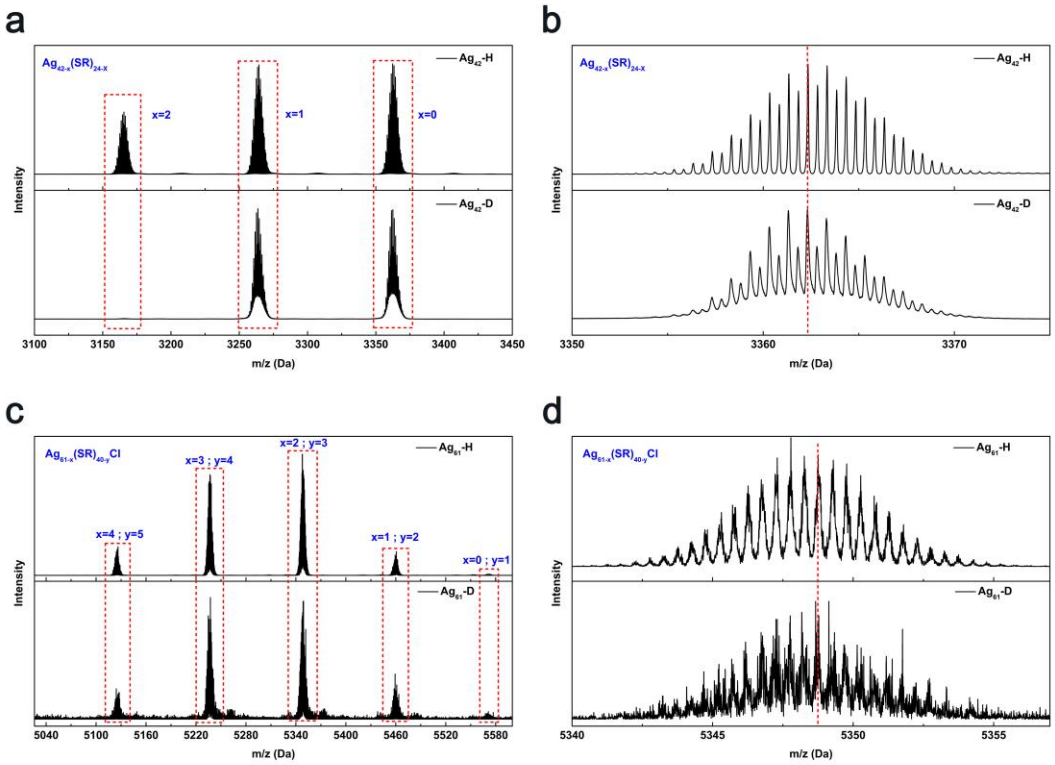

Figure S17. ESI-MS spectra of (a) **Ag_{42}-H** and **Ag_{42}-D** (**Ag_{42}-H** represents the use of $NaBH_4$ as reducing agent, and **Ag_{42}-D** represents the use of $NaBD_4$ as reducing agent), x = 0, x = 1, x = 2 were assigned to $[Ag_{42}(SC_4H_9)_{24} + CH_3OH + Na^+ + H^+]^{2+}$, $[Ag_{41}(SC_4H_9)_{23} + CH_3OH + Na^+ + H^+]^{2+}$ and $[Ag_{40}(SC_4H_9)_{22} + CH_3OH + Na^+ + H^+]^{2+}$, respectively; (b) Enlarged view of **Ag_{42}-H** and **Ag_{42}-D** at x = 0; (c) **Ag_{61}-H** and **Ag_{61}-D**, x = 0, x = 1, x = 2, x = 3, x = 4 were assigned to $[Ag_{61}(SC_6H_{11})_{39}Cl + H^+]^{2+}$, $[Ag_{60}(SC_6H_{11})_{38}Cl + CH_3OH + H^+]^{2+}$, $[Ag_{59}(SC_6H_{11})_{37}Cl + CH_3OH + H^+]^{2+}$, $[Ag_{58}(SC_6H_{11})_{36}Cl + CH_3OH + H^+]^{2+}$, $[Ag_{57}(SC_6H_{11})_{35}Cl + CH_3OH + H^+]^{2+}$, respectively; (d) Enlarged view of **Ag_{61}-H** and **Ag_{61}-D** at x = 2.

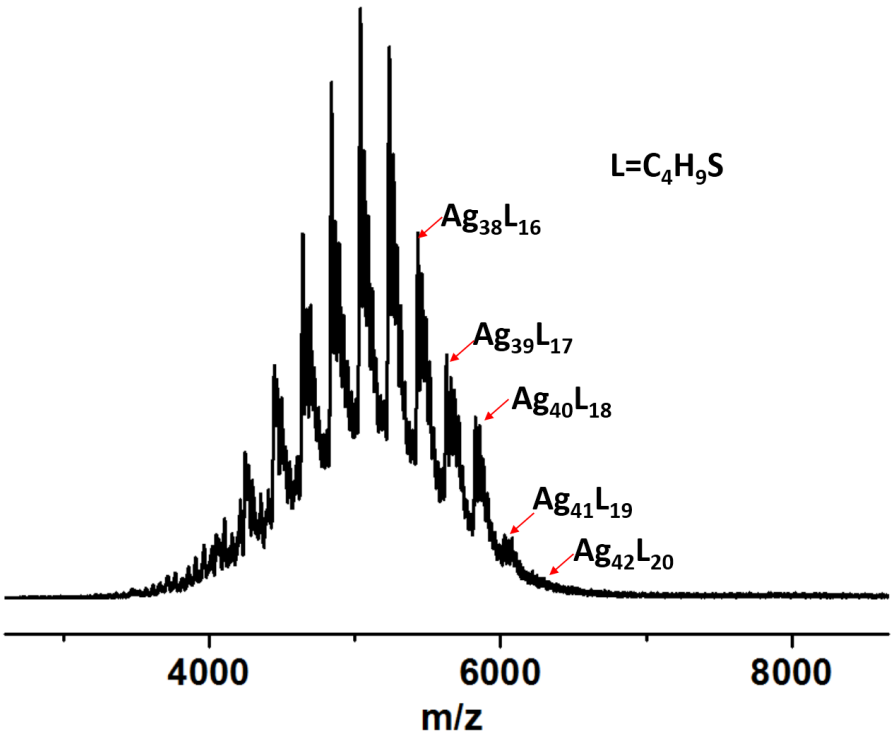

Figure S18. MALDI-MS spectrum of **Ag_{42}** (**Ag_{42}** crystal soluble in CH_2Cl_2 solvent) in linear positive ionization mode using DCTB as matrix. The peak with the largest molecular weight corresponds to $Ag_{42}(C_4H_9S)_{20}$. And each of two adjacent peaks separated m/z = 198.0 Da, assigned to Ag-SC_4H_9.

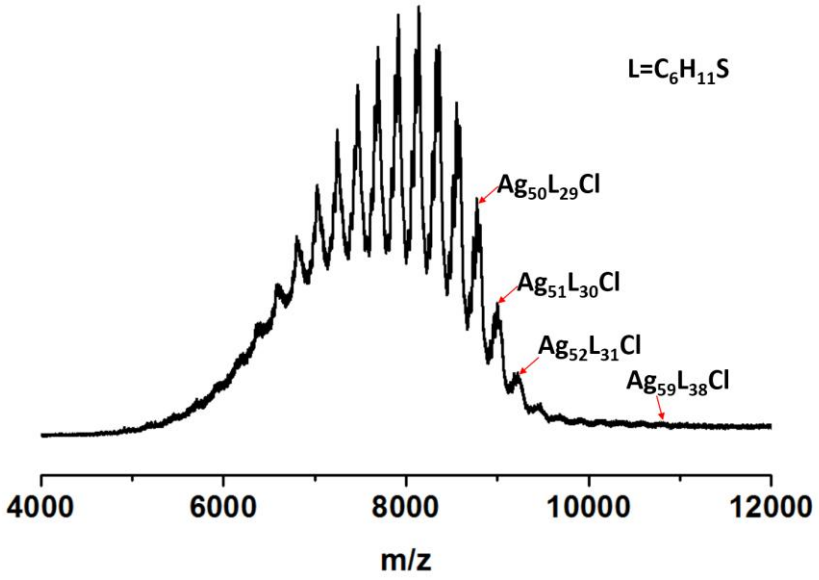

Figure S19. MALDI-MS spectrum of **Ag_{61}** (**Ag_{61}** crystal soluble in CH_2Cl_2 solvent) in linear positive ionization mode using DCTB as matrix. The peak with the largest molecular weight corresponds to $Ag_{59}(C_6H_{11}S)_{38}Cl$. And each of two adjacent peaks separated m/z = 221.9 Da, assigned to $Ag\text{-}SC_6H_{11}$.

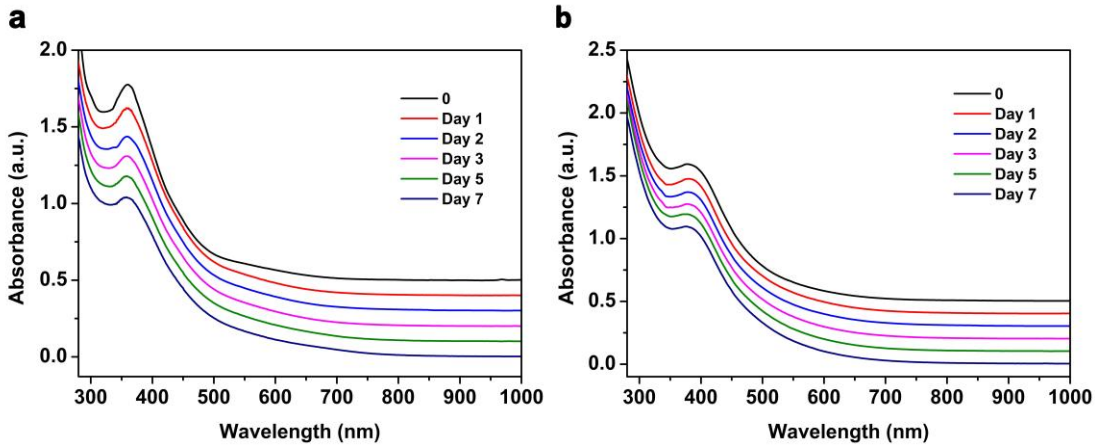

Figure S20. Thermostability of (a) **Ag_{42}** and (b) **Ag_{61}** at room temperature.

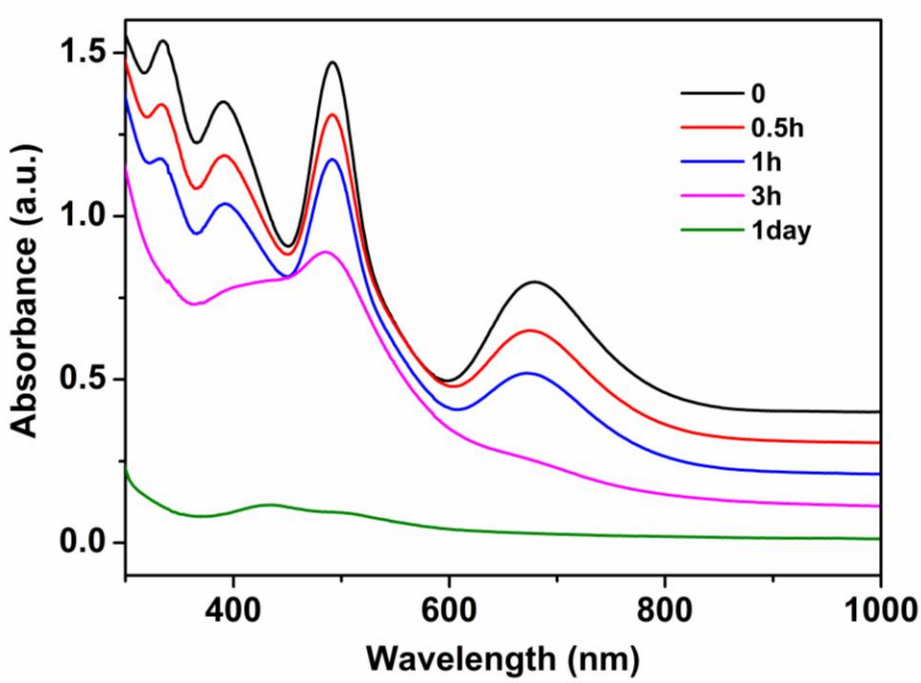

Figure S21. Thermostability of $[Ag_{25}(SPhMe_2)_{18}]^-$ at room temperature.

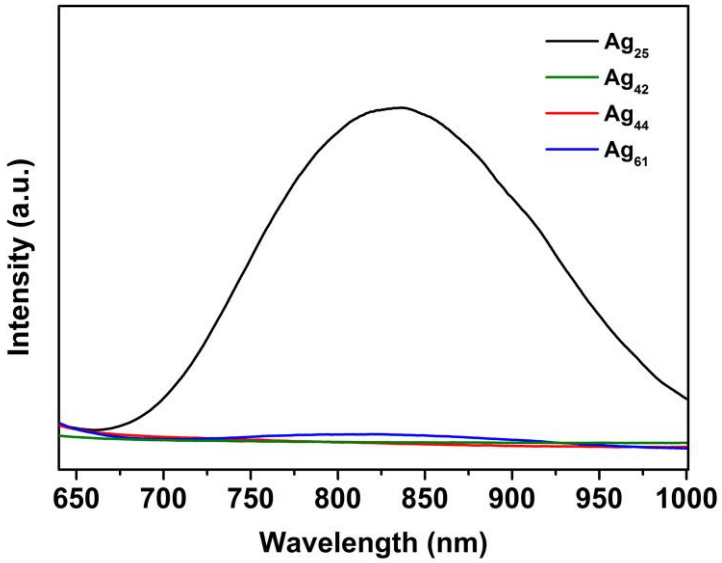

Figure S22. Photoluminescence spectra of $Ag_{25}(SR)_{18}^-$, $Ag_{42}(SR)_{24}$, $Ag_{44}(SR)_{30}^{4-}$ and $Ag_{61}(SR)_{40}Cl$ using dichloromethane as solvent (excited at 365nm).

Table S1 Crystal data and structure refinement for $Ag_{42}(SC_4H_9)_{24}$

Identification code	$Ag_{42}(SC_4H_9)_{24}$	
Empirical formula	$C_{50.50}H_{113}Ag_{21}Cl_5S_{12}$	
Formula weight	3547.64	
Temperature	173 K	
Wavelength	0.71073 Å	
Crystal system	Orthorhombic	
Space group	P222	
Unit cell dimensions	a = 19.018(2) Å	α = 90°.
	b = 19.679(2) Å	β = 90°.
	c = 26.250(3) Å	γ = 90°.
Volume	9824.2(18) $Å^3$	
Z	4	
Density (calculated)	2.399 Mg/m^3	
Absorption coefficient	4.494 mm^{-1}	
F(000)	6720	
Theta range for data collection	0.776 to 25.999°.	
Index ranges	-24<=h<=24, -25<=k<=19, -33<=l<=32	
Reflections collected	71886	
Independent reflections	19208 [R(int) = 0.0478]	
Completeness to theta = 25.242°	99.9 %	
Absorption correction	Semi-empirical from equivalents	
Max. and min. transmission	0.7455 and 0.5628	
Refinement method	Full-matrix least-squares on F^2	
Data / restraints / parameters	19208 / 336 / 875	
Goodness-of-fit on F^2	1.029	
Final R indices [I>2sigma(I)]	R1 = 0.0866, wR2 = 0.2111	
R indices (all data)	R1 = 0.1157, wR2 = 0.2415	
Absolute structure parameter	0.028(15)	
Extinction coefficient	n/a	
Largest diff. peak and hole	3.463 and -4.237 $e.Å^{-3}$	

Table S2. Crystal data and structure refinement for $Ag_{61}(SC_6H_{11})_{40}Cl$

Identification code	$Ag_{61}(SC_6H_{11})_{40}Cl$	
Empirical formula	$C_{242}H_{444}Ag_{61}Cl_5S_{40}$	
Formula weight	11393.67	
Temperature	296.15 K	
Wavelength	0.71073 Å	
Crystal system	Orthorhombic	
Space group	$P2_12_12_1$	
Unit cell dimensions	a = 22.088(11) Å	α = 90°.
	b = 39.696(19) Å	β = 90°.
	c = 39.85(2) Å	γ = 90°.
Volume	34941(30) $Å^3$	
Z	4	
Density (calculated)	2.166 Mg/m^3	
Absorption coefficient	3.641 mm^{-1}	
F(000)	21952	
Crystal size	0.12 x 0.1 x 0.03 mm^3	
Theta range for data collection	2.115 to 29.825°.	
Index ranges	-29<=h<=30, -33<=k<=55, -55<=l<=45	
Reflections collected	229686	
Independent reflections	97131 [R(int) = 0.0802]	
Completeness to theta = 25.242°	98.8 %	
Absorption correction	Semi-empirical from equivalents	
Max. and min. transmission	0.7552 and 0.258	
Refinement method	Full-matrix-block least-squares on F^2	
Data / restraints / parameters	97131 / 3132 / 3133	
Goodness-of-fit on F^2	1.085	
Final R indices [I>2sigma(I)]	R1 = 0.0897, wR2 = 0.2160	
R indices (all data)	R1 = 0.1429, wR2 = 0.2502	
Absolute structure parameter	0.073(14)	
Extinction coefficient	n/a	
Largest diff. peak and hole	6.451 and -3.765 $e.Å^{-3}$	